The Journal of Adhesion
Publication details, including instructions for authors and subscription information:
http://www.tandfonline.com/loi/gadh20

Buckling of an Adhesive Polymeric Micropillar

Dadhichi R. Paretkar [a], Michael D. Bartlett [b], Robert McMeeking [a c d], Alfred J. Crosby [b] & Eduard Arzt [a]

[a] INM-Leibniz Institute for New Materials, Functional Surfaces Group, and Saarland University, Saarbruecken, Germany

[b] Polymer Science and Engineering Department, University of Massachusetts, Amherst, Massachusetts, USA

[c] Department of Mechanical Engineering and Materials Department, University of California, Santa Barbara, California, USA

[d] School of Engineering, University of Aberdeen, King's College, Aberdeen, Scotland

Published online: 26 Nov 2012.

To cite this article: Dadhichi R. Paretkar, Michael D. Bartlett, Robert McMeeking, Alfred J. Crosby & Eduard Arzt (2013) Buckling of an Adhesive Polymeric Micropillar, The Journal of Adhesion, 89:2, 140-158, DOI: 10.1080/00218464.2013.731941

To link to this article: http://dx.doi.org/10.1080/00218464.2013.731941

The Journal of Adhesion, 89:140–158, 2013

ISSN: 0021-8464 print/1545-5823 online
DOI: 10.1080/00218464.2013.731941

Taylor & Francis
Taylor & Francis Group

Buckling of an Adhesive Polymeric Micropillar

DADHICHI R. PARETKAR[1], MICHAEL D. BARTLETT[2], ROBERT McMEEKING[1,3,4], ALFRED J. CROSBY[2], and EDUARD ARZT[1]

[1]*INM-Leibniz Institute for New Materials, Functional Surfaces Group, and Saarland University, Saarbruecken, Germany*
[2]*Polymer Science and Engineering Department, University of Massachusetts, Amherst, Massachusetts, USA*
[3]*Department of Mechanical Engineering and Materials Department, University of California, Santa Barbara, California, USA*
[4]*School of Engineering, University of Aberdeen, King's College, Aberdeen, Scotland*

Adhesion and buckling of single PDMS micropillars were investigated as a function of compressive preload. The micropillars had diameters of 10, 12, 14, and 20 μm and aspect ratios of 1 to 3.3. Adhesion generally increased with a decrease in the aspect ratio. A dependence of pull-off strength on the compressive preload stress was found for micropillars that underwent buckling. When buckling was reversible, tip contact recovered upon unbuckling, which resulted in only a slight reduction of adhesion. In situ observation studies identified irreversible buckling, i.e., lack of tip-contact re-formation, resulting in adhesion loss. It is concluded that the edge radius of the tip, which acts as a circumferential crack, controls adhesion. Fibril buckling is found to be broadly consistent with the predictions of Euler buckling theory.

KEYWORDS Aspect ratio; Fibril buckling; Gecko adhesion; Reversible adhesion; Single fibirl; Tip shape

Received 3 June 2012; in final form 13 August 2012.

One of a Collection papers honoring Wulff Possart, the receipent in February 2012 of *The Adhesion Socity Award for Excellence in Adheion Science, Sponsored by 3M*.

Address correspondence to Eduard Arzt, INM-Leibiniz Institute for New Materials, Functional Surfaces Group, and Saarland University, Campus D 22, 66123 Saarbruecken, Germany. E-mail: eduard.arzt@inm-gmbh.de

INTRODUCTION

Bioinspired reversible adhesive surfaces generally consist of arrays of hundreds or thousands of micropillars (or fibrils) on a soft backing as summarized in recent reviews [1–3]. These adhesives are tested by compressively loading them against a probe surface and by retracting them in tension until detachment occurs. Numerous studies have investigated the influence of sample characteristics on the adhesion mechanisms, *e.g.*, sample compliance [4,5], backing layer compliance [6–8], tip shape of fibrils [9,10], fibril radius and aspect ratio (AR) [11,12], and orientation of the fibrils with respect to probe [13] or roughness of the probe [14–16]. The impression these results create is that different factors influence the adhesion mechanisms differently and often their combined influence is complex.

An inherent complexity of fibrillar surfaces is the multiplicity of contact formation and separation. Modelling a single fibril [17,18] or the interactions among, at best, a few during attachment and detachment [19], provides only a qualitative picture of the intricate, multi-contact phenomena. The situation is further complicated by the details of how loading and unloading is carried out, *e.g.*, the presence or absence of shearing motion and frictional effects [20] or the type of probe (flat/spherical) used [13]. In addition, micropillar fabrication leads to variations in their dimensions and to defects on their surfaces. This introduces stochastic effects into the phenomena of contact and adhesion when many fibrils are involved [21].

An important outcome of these observations and those of others [22,23] is that the collective interactions of many fibrils provides little insight into phenomena occurring at the single fibril level. Such phenomena include attachment and buckling under compression, fibril tip detachment during buckling, tip re-attachment upon unbuckling during unloading, and full detachment at the adhesion limit, all of which contribute to the system's adhesive strength. The present study focuses on investigation of these mechanisms for a single polydimethylsiloxane (PDMS) micropillar. Previous experimental studies on single micropillar adhesion [12] or buckling [23] use, fibrils with much larger dimensions than the micro-scale of current interest. The present study investigates single micropillars having diameters of 10, 12, 14, and 20 μm and heights of 20 and 33 μm. The effects on fibril adhesion and buckling associated with an increase in the applied compressive preload were studied with the aim of extending our understanding of adhesion and buckling in bioinspired adhesives.

EXPERIMENTAL

Single micro-scale pillars with heights, h, of 20 and 33 μm with diameters, d, equal to 10, 12, 14, and 20 μm in each case were obtained. These PDMS

micropillars were fabricated using photolithography and soft molding techniques. Lithography masks were designed such that a single hole within a square centimeter area was obtained by the use of a negative tone SU-8 resist.

Photolithography

SU-8 resists 2010 and 2025 (Micro Resist Technology, Berlin, Germany) were spin-coated on cleaned Si wafers (100 orientation, Crystec Berlin, Germany) to thicknesses of 20 and 33 μm, respectively (Suss Microtech AG, Garching, Germany). The general photolithography steps for SU-8 resists were followed [24]. These steps of soft-bake, exposure, post-exposure bake, and development were further optimized for obtaining single holes in SU-8, (Table 1).

Soft Moulding of PDMS Single Micropillars

The PDMS (10:1, prepolymer to cross-linker) mixture was prepared using the Dow Corning® (Dow Corning Corp. Midland, MI, USA) Sylgard® 184 kit. The mixture was degassed and poured on silanized SU-8 masters. Upon curing at 75°C for at least 14 h the crosslinked PDMS was carefully peeled-off from the SU-8 masters. Single micropillars of two different heights and four different diameters were obtained. This led to a range of aspect ratios (AR) from 1 to 3.3. The PDMS backing of the micropillars was about 2 to 3 mm thick, which is two to three orders of magnitude greater than the micropillar dimensions.

Characterization of Single Micropillars

SEM micrographs of some low and high AR single micropillars are shown in Fig. 1. Sometimes surface wrinkles in the PDMS backing were observed [Fig. 1 (c) and (d)] due to release of stress during moulding between the stiff SU-8 and the soft PDMS. Some pillars appeared to be slightly bent in SEM micrographs.

Defects such as bent pillars are known to occur during the lithography process and may be attributed to a non-uniformity in UV exposure and

TABLE 1 Photolithography Process for Obtaining Single Cylindrical Holes in SU-8 Resists

Process steps	SU-8 2010	SU-8-2025
1. Soft-bake	95°C for 5.5 min	95°C for 5.5 min
2. UV exposure (15 mW/cm^2)	14.3 s	19.3 s
3. Post-exposure bake	95°C for 5.5 min	95°C for 5.5 min
4. Development	4 min	4.5 min

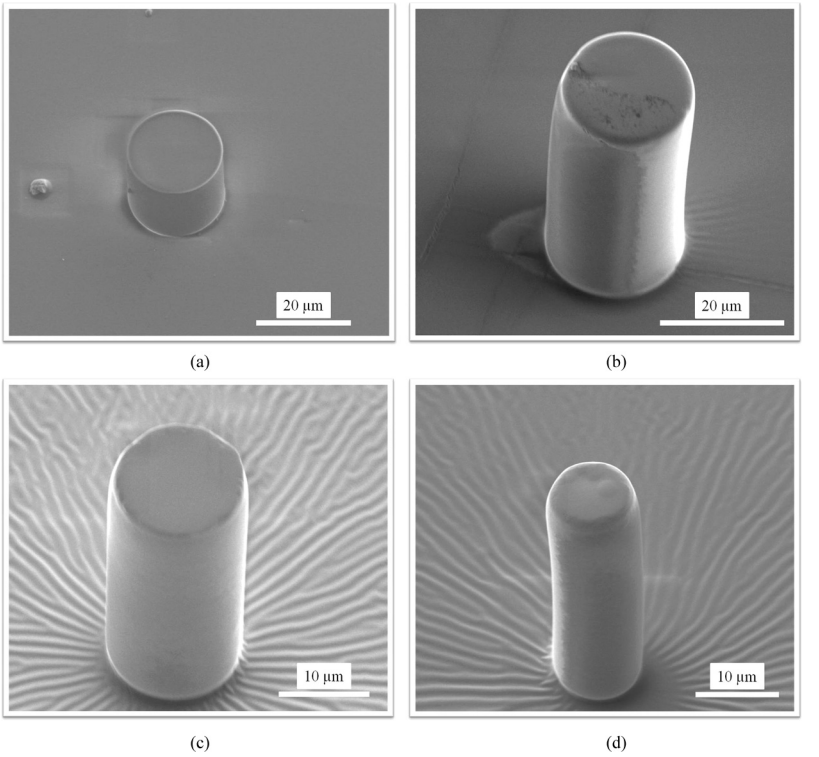

FIGURE 1 SEM images of low aspect ratio (AR) single micropillars with diameter $d = 20\,\mu m$ and (a) AR 1, height $h = 20\,\mu m$; (b) AR 1.6, height $h = 33\,\mu m$. High AR single micropillar: (c) AR 2.3, $h = 33\,\mu m$, and $d = 14\,\mu m$; (d) AR 3.3, $h = 33$, and $d = 10\,\mu m$.

thickness variations in SU-8 films [11]. A given mould provided between 9 and 16 single fibril specimens, several of which had straight micropillars. We selected the straight ones for testing and disposed of the bent ones.

The *edge radius* was estimated as demonstrated in the SEM image inserted in table below; see sketch of the pillar tip in the inset in Table 2.

The heights of the micropillars were confirmed optically by white light interferometry (Fig. 2).

Adhesion Testing

The adhesion experiments were conducted on a custom designed instrument *Contact Adhesion Testing Device* (Fig. 3).

The device consisted of a piezo-controlled linear actuator (Burleigh® Inchworm nanopositioner, Newton, NJ, USA) controlling the travel of the sample, a cantilever-based capacitance force transducer, and a fully automated, inverted optical microscope Axiovert™ 200 M (Carl Zeiss GmbH, Oberkochen, Germany) to visualize the contact interface during the test.

TABLE 2 Estimated Edge Radii of Single Micropillars from SEM Images

Single micropillar	Edge radius [μm] $h = 20$	Edge radius [μm] $h = 33$	
$d = 10$	~0.64–0.69	~0.69–0.75	The edge radius was measured on the SEM image. Inset shows the method of determination of edge radius. The radius was measured at several locations to determine the range listed on the left.
$d = 12$	~0.63–0.68	~0.74–0.8	
$d = 14$	~0.57–0.62	~0.8–1	
$d = 20$	~0.76–0.8	~0.72–0.79	

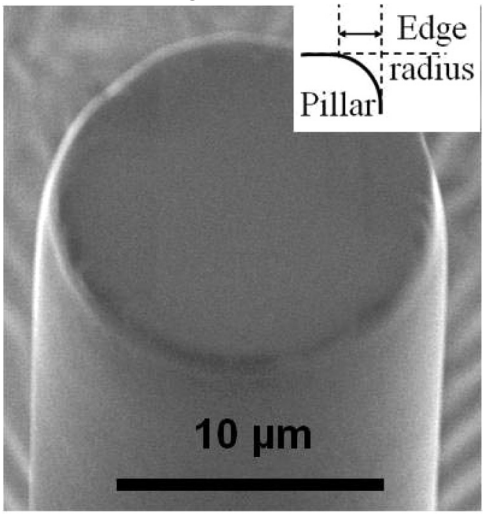

The total instrument compliance, which was mainly due to the cantilever, was 3925 μm/N (at least 10 times as stiff as than the sample). Each component was controlled through custom-written software within a National Instruments Labview™ environment (National Instruments Corp., Austin, TX USA). The test procedure involved attaching the single fibril PDMS sample to the cantilever, which in turn was mounted on the linear actuator.

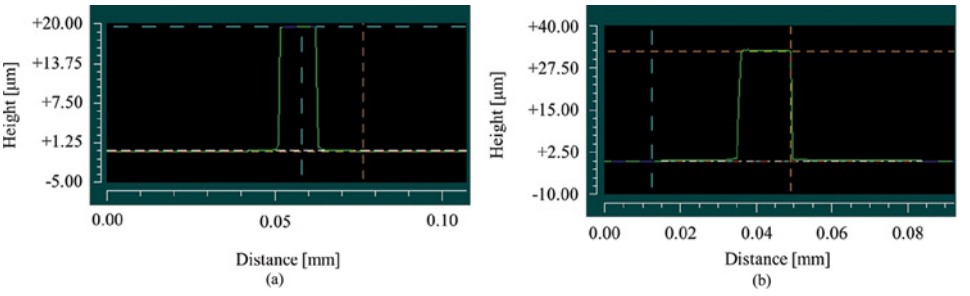

FIGURE 2 White light interferometry images of single micropillar profiles: (a) height $h = 20$ μm, diameter $d = 10$ μm, (b) $h = 33$ μm, $d = 14$ μm (color figure available online).

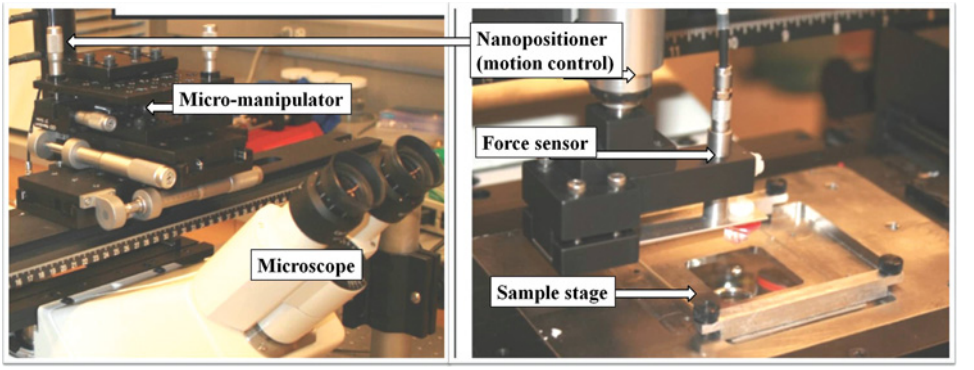

FIGURE 3 Contact adhesion testing device (images courtesy C. Davis) (color figure available online).

Adhesion was tested against a glass plano-convex lens of diameter 6 mm and radius of curvature 15 mm (Edmund Optics™, Barrington, NJ, USA) and a glass hemisphere (diameter 1 mm) fixed on the stage of the inverted optical microscope. The single fibril was compressed against the glass probe to various levels of preload stress (maximum of the magnitude of compressive load divided by the undeformed pillar cross-section area) and subsequently retracted until pull-off. Adhesion of the micropillar was recorded as the pull-off strength (maximum tensile load—or pull-off force—divided by the undeformed pillar cross-section area). During contact and separation, the displacement of the sample, the applied force, and the contact area were continuously monitored and recorded. All experiments were performed at room temperature, and the displacement rate of the sample was $0.89 \pm 0.04\,\mu m/s$.

RESULTS

1. Pull-Off Strength as a Function of Compressive Preload Stress

   Fig. 4(a) shows the pull-off strength as a function of the preload stress for single micropillars with height $h = 20\,\mu m$ having different aspect ratios (AR). Tests were carried out using the 6-mm diameter plano-convex glass probe. Increasing the preload stress had no significant effect on their pull-off strengths [Fig. 4(a)].

2. Buckling as a Function of Preload Stress

   For the micropillars with $h = 20\,\mu m$ no buckling was observed for the range of preload stress used. The taller, $h = 33\,\mu m$ micropillar samples with diameters of 10, 12, and 14 μm buckled at higher preload stress (0.8–2 MPa). Buckling was visible during the pillar observations and corresponded to

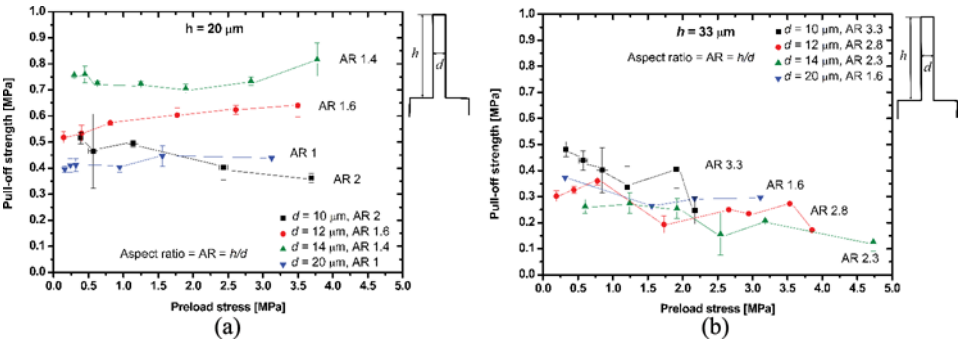

FIGURE 4 Pull-off strength as a function of preload stresses (i.e., maximum of the magnitude of compressive stress) for single micropillars with (a) height $h = 20\,\mu m$ and (b) $h = 33\,\mu m$ having various aspect ratios (AR). Error bars indicate the variations in the measured stress/strength from at least three test repetitions (color figure available online).

a slight lowering of adhesion. The contact mechanisms for both the low and high preload cases are presented here. Micropillars with AR 3.3 ($h = 33$ and $d = 10\,\mu m$) are taken as representative for this purpose.

Low Preload: No Buckling

Low preload stress ($\leq 0.6\,MPa$) applied using the 6-mm diameter plano-convex glass probe did not cause buckling of the AR = 3.3 micropillar (Fig. 5). Inset snapshots are provided above the plot and show the top view of the pillar-probe interface, revealing the characteristics of the contact. The time at which the snapshot was recorded is given in each inset. Insets 1 and 5 show the pillar tip not in contact with the probe (light gray circular spot) before and after the adhesion test. Insets 2 and 3 show the pillar tip in full contact with the micropillar under compression (dark gray circular spot). Inset 4 shows the pillar tip in full contact with the probe prior to its detachment with the micropillar under tension. The pull-off strength was $0.44 \pm 0.04\,MPa$.

High Preload: Reversible Buckling

Figure 6 shows that a high preload stress of 1.25 MPa caused *reversible* buckling for the same micropillar-probe combination as above. Insets in Fig. 6 and the accompanying side view sketch in Fig. 7 shows the micropillar deformation for the high preload case.

During *loading*, the applied compression caused the pillar tip to come in full contact with the probe (inset 1). Insets 2 and 3 show a transition from a complete top face contact (dark gray circular spot, inset 2) to partial side contact (dark-gray moon shape indicates fibril edge while top face with lighter gray areas indicates fibril side, inset 3). The micropillar formed a hook shape

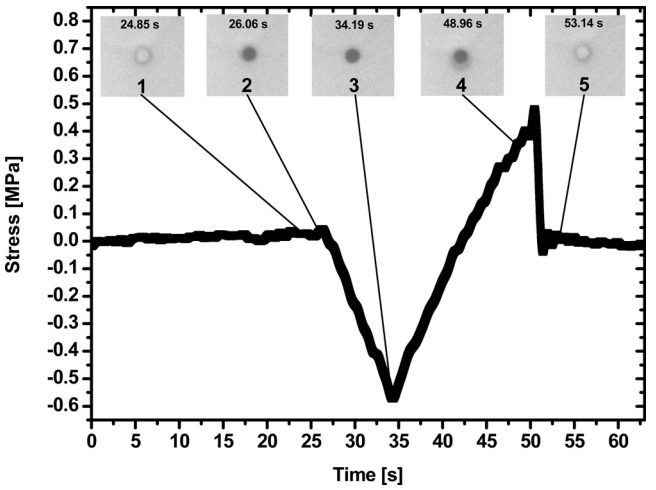

FIGURE 5 Evolution of applied stress in time during an adhesion test for a 10-μm diameter, 33-μm high (AR 3.3) single micropillar. The fibril is compressed at constant velocity against the 6-mm plano-convex lens to a relatively low preload stress of 0.6 MPa and then retracted at constant velocity. Compressive stress is negative and tensile stress is positive. No buckling is observed. Insets show the top view of the pillar-probe interface at the time indicated. The light-dark rings correspond to the thicker contour of the pillar viewed out of focus.

at the stress of ~0.75 MPa around t = 20 s (sketch 3, Fig. 7). This change from tip to side contact was accompanied by a decrease in compressive stress indicating *buckling*. Inset 4 shows the pillar partially folded onto itself at maximum compressive load. In the side contact state the darker gray region

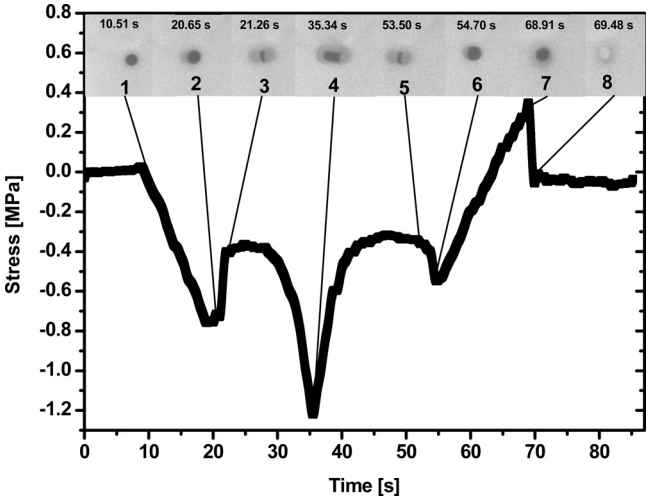

FIGURE 6 Same as Fig. 5, but for a higher preload stress of 1.25 MPa. Buckling is observed but is partially reversed on retraction, resulting in recovery of some adhesion. See text for details.

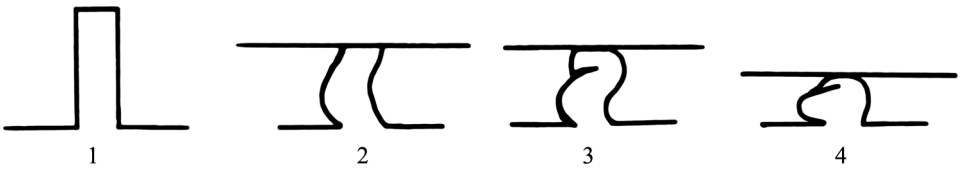

FIGURE 7 Schematic of the side view of a single micropillar corresponding to different stages of increasing applied compressive stress magnitude (sketches 1 to 4 correspond to insets 1 to 4 in Fig. 6, respectively).

indicates the fibril tip retaining partial contact (sketch 4). Due to elastic strain during compression, the area of the fibril tip has been increased.

During *unloading*, the elastic strain of the tip reversed (from inset 4 to 5). Further reduction in compressive stress returned the fibril to almost exactly the same shape it had when it first buckled (inset 5). Insets 5 and 6 show the fibril straightening from hook-shape back to full tip contact at around $t = 55$ s, indicating *reversal of buckling* or *unbuckling*. This event was accompanied by an increase in the compressive stress magnitude consistent with unbuckling. Inset 6 shows the fibril tip in full contact and being pulled into tension towards detachment. Insets 7 and 8 capture the fibril tip immediately prior to and after detachment, respectively.

The pull-off strength in this case of *reversible buckling* was 0.33 ± 0.08 MPa. Note that this value is about 75% of the value without buckling (low preload case, 0.44 ± 0.04 MPa). Similar observations were made for other micropillars that showed reversible buckling. For example, pull-off strength dropped from 0.35 MPa to below 0.2 MPa for the 12-μm diameter ($h = 33$ μm) micropillar when the preload stress exceeded 1 MPa causing reversible buckling [Fig. 4(b)]. Such a decrease is attributed to an incomplete recovery of the contact after unbuckling.

Micropillar Slippage: Irreversible Buckling

When a hemispherical glass probe (radius of curvature 0.5 mm) was used instead of the plano-convex lens (radius of curvature 15 mm), the micropillars slipped during the unloading stage after high preload stress. Such slippage occurred only for buckled micropillars during unloading from a preload higher than the critical buckling stress.

Figure 8 shows the stress *versus* time plot for an AR 3.3 micropillar tested against the hemispherical probe (radius of curvature 0.5 mm) with accompanying snapshots. During *loading* to high preload stress, inset 1 captures the micropillar in a hook-shape just after buckling, as in the previous case. Further increase in compressive load resulted in a slight bias of the hook-shape towards the right, inset 2. This bias may be due to the step-like motion of the piezo controller. At maximum compressive preload, the gap between

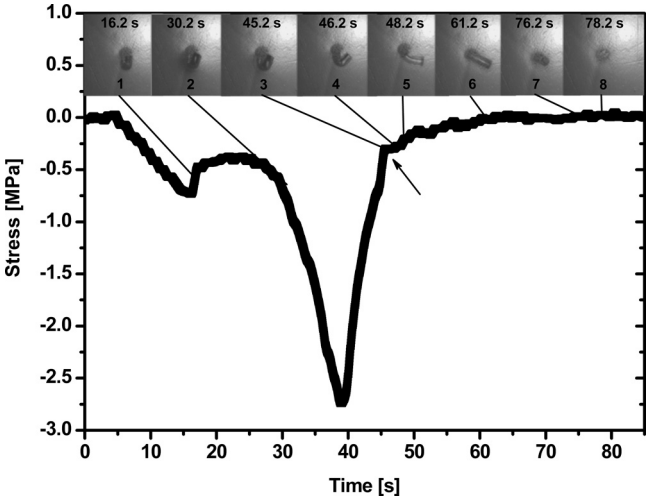

FIGURE 8 Evolution of applied stress in time during an adhesion test for a 10-μm diameter, 33-μm high (AR 3.3) single micropillar. The fibril is compressed at constant velocity against the 1-mm diameter glass hemisphere to a relatively high preload stress of 2.8 MPa and then retracted at constant velocity. Insets show the top view of the pillar-probe interface at the time indicated.

the probe and the backing layer had closed so that the folded fibril was pinned between the probe and the backing layer.

During *unloading* the exact reversal in fibril configuration was not observed. As the load relaxed, the fibril tip slipped towards the bias direction collapsing sideways (insets 3 and 4). The stress-time plot showed a distinct change of slope around 44 s (arrow, inset 3) coinciding with fibril collapse. The collapsed fibril adopted a single layer folded V-shape different from the double layer folded hook-shape. The V-shaped fibril was pinned under reducing compressive load between the probe and the backing layer (inset 4). Further reduction in compressive load magnitude resulted in the fibril straightening out as the probe retracted (insets 6 and 7). The corresponding change in stress was negligible. Finally, the micropillar detached without adhesion (inset 8). Similar behaviour was observed for other fibrils ($d = 10$, 12, and 14 μm with $h = 33$ μm), which showed a buckling instability at high preloads, when tested using the hemispherical probe.

DISCUSSION

Aspect Ratio

All micropillars having a height of 20 μm showed a decrease in pull-off strengths with an increase in fibril aspect ratio (with the exception of AR 1) when tested with the 6-mm diameter plano-convex lens, see Fig. 4(a).

These fibrils were not subject to buckling. In addition, micropillars having a given diameter exhibit decreasing adhesive strength as their height, *i.e.*, AR, is increased. In many cases, the effect is due to buckling that sets in for the fibrils with higher AR when subject to higher preload stress [Fig. 4(b)]. However, it is notable that the trend is the same when AR is increased for those fibrils that do not buckle because the preload stress is below the critical buckling level, *i.e.*, the pull-off force decreases with increasing AR even in cases where no buckling is involved.

These results are broadly consistent with the experimental data of Aksak et al. [12] for single fibrils attached to a stiff probe over their entire tip-face area. However, they are in contrast to some results obtained with arrays of micropillars, where an increase in AR led to an increase in adhesive strength attributed to an increase in compliance [22,25]. On the other hand, some experiments with micropillar arrays have led to results in which the pull-off force decreased if the compliance increase was due to the backing layer [6]. It has been argued that the higher strain energy stored in longer, high AR micropillars leads to an increase in pull-off force compared with that for shorter fibrils of the same diameter [26,5]. The reasoning is that the additional strain energy is lost upon detachment, causing additional dissipated work that has to be done on the fibril to cause it to detach. However, this model is not consistent with our data for single microfibrils and those of Aksak *et al.* [12] for the same situation. Thus, the situation is ambiguous. Indeed, a contrasting argument can be given that fibrils that are more compliant, as is the case of a higher AR fibril compared with a lower AR one at fixed diameter, are more prone to be detached unstably at a lower stress because their behaviour is closer to that experienced under load control in contrast to displacement control [27].

Furthermore, we note the dominant influence of the details of fibril tip shape, *e.g* [9]., and infer from this that the edge radius of the micropillars we tested must play an important role in determining the pull-off force in our tests of single micropillars. We deduce that the edge radius of our micropillars is effectively a circumferential crack around the perimeter of the tip when it is adhered to the probe. This leads to relatively easy peeling of the tip when it detaches, subject to the balance between strain energy released and adhesion work required. The plots of pull-off strengths as a function of the edge radii of different micropillars (see Table 2) point out that the pull-off strengths in our data for unbuckled fibrils, and for those buckled under compression by the plano-convex lens, are controlled by the edge radius, with larger edge radii leading to lower pull-off strengths and *vice versa* (Fig. 9). A detailed model for detachment controlled by an edge radius can be developed, but given the complexities of sticking friction during adhesion, mode-mixity, and the effect of the compliance of the backing layer, we prefer to leave its development to future work. All aspects of adhesion and fracture mechanics, however, suggest that the contribution from the edge radius is significant.

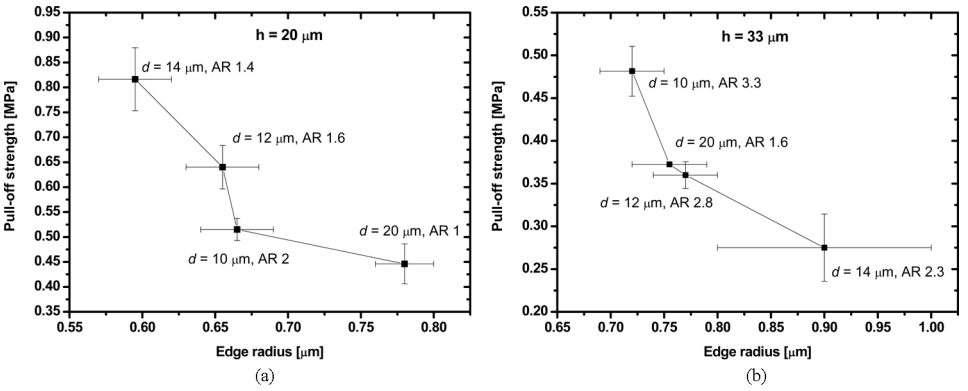

FIGURE 9 Pull-off strength as a function of edge radius of the micropillar for different aspect ratios (AR) having (a) $h = 20\,\mu m$ and (b) $h = 33\,\mu m$.

Higher AR fibrils are known to be more compliant than those with lower AR at fixed diameter [28]. This feature is confirmed for all but the 14-μm diameter fibrils in Fig. 10(a), which is a plot of experimentally measured compliance *versus* fibril diameter for our single micropillar specimens subject to tension prior to pull-off. The compliance is defined as the inverse of the slope of the force-displacement curve. In almost all cases, the compliance of higher AR fibril specimens is greater than that of the lower AR case at the same micropillar diameter, as expected, and consistent with the results of Aksak *et al.* [12]. Thus, both an increase in adhesion and an increase in stiffness of the specimen were observed when the fibril AR was reduced at fixed diameter, consistent with the results of Aksak *et al.* [12]. However, compliance is influenced by both geometry and material elastic modulus, and the data in Fig. 10(a) do not conform to predictions of compliance based on a

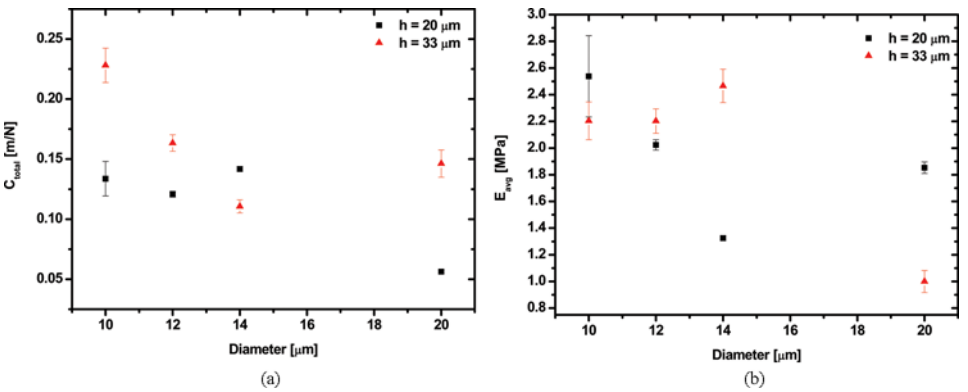

FIGURE 10 Elastic response of the micropillars: (a) Measured compliance (C_{total}) from the tensile regime of the force-displacement plots for all single micropillar specimens; (b) Calculated average elastic modulus (E_{avg}) (color figure available online).

common value of elastic modulus. The most obvious example of this is the case of the 14-μm diameter fibril, where the shorter one is more compliant than the longer one. To investigate the relative importance of geometry and elastic modulus in determining the compliance, we convert the data for compliance (C_{total}) in Fig. 10(a) to an inferred value of the average elastic modulus (E_{avg} for PDMS), as follows.

The compliance of the pillar and the backing are considered to be additive such that the effective compliance is $C_{total} = C_{pillar} + C_{backing}$ [19].

The average elastic modulus was calculated using the experimentally measured compliance following the procedure of Guidoni *et al.* [19], with the use of

$$E_{avg} = \left[\frac{h}{(1-\nu^2)r} + \frac{16}{3\pi}\right]\frac{(1-\nu^2)}{\pi r C_{total}}, \tag{1}$$

where h and r are the fibril height and radius, respectively, and ν is Poisson's ratio (~0.5). The calculated average elastic modulus is presented, for all single micropillar specimens, in Fig. 10(b). The results show that when the pillar diameter was reduced, keeping the height constant, a general *increase* in average modulus was measured. The single micropillar strains were between 14–17% for which we do not expect non-linear behaviour of PDMS.

We also note the scatter in the data, which can be attributed to different sources: the batch-to-batch variation in the modulus of the PDMS, which can arise from slight changes in cure temperature and mix ratio [29], or variations in heat transfer in the different molds that caused local parts to cure at slightly different temperatures, leading to network heterogeneities.

Preload

Results in Fig. 4(a) are broadly independent of preload stress, and those in Fig. 4(b) are only weakly dependent on it. In the latter case, the dependence on preload can be attributed to the buckling of all micropillars with $h = 33\,\mu m$, except AR 1.6, that occurred at high preloads [Fig. 4(b)].

Our *in situ* observations showing the fibril-probe interface contact (insets in Fig. 6) helped in the understanding of measured adhesion values. The hook-shape that the fibril adopted after buckling against the plano-convex lens remained stable throughout the time between buckling and unbuckling. This is because the buckled fibril was severely constrained between the plano-convex probe and the backing layer, with little opportunity to move relative to the probe and reconfigure its shape. In the hook-shape, there was always some fraction of the fibril tip that remained in adhesive contact with the probe, even if much of the top-face had detached due to buckling. The fact that there is a residual area of the tip that remains in contact with the probe facilitates easy reattachment to the probe when it is

retracted and the fibril unbuckles. Thus, the use of a probe with a large radius of curvature, the stiffness of the instrumentation, the size and AR of the fibrils, and the presence of compressive stress allowed for an almost complete reattachment of the fibril tip to the probe. Indeed, the images in the insets in Fig. 8 suggest that the fibril top-face completely reattached to the probe when the micropillar underwent unbuckling. However, the contact configuration after buckling reversal was somewhat different from that established after the fibril and probe were first brought into contact. As a consequence of such hysteresis in adhesion, the shape and size of the features that controlled the pull-off force were somewhat different, leading to a slight reduction in the resulting pull-off force.

Slippage of Micropillars

In contrast, when a 1-mm diameter hemisphere was used as the probe, the buckled fibril had additional freedom of motion because of the smaller radius of curvature of the probe (Fig. 8). The strain energy of the fibril tends to introduce some irreversibility into the motion of the fibril tip relative to the probe as the system seeks a path that reduces its potential energy. As a consequence, the fibril tip was able to rotate and twist from under the apex of the probe to a location where there was a larger gap between the probe and the backing layer. This also involved the complete detachment of the fibril tip from the probe. The buckled fibril was, therefore, able to slide relative to the probe, rotate and twist until it had partially released its stored strain energy, and lay prone on its sides. The fibril rotation was also very likely induced by some inadvertent back-and-forth sideways motion of the probe when the nano-positioner controlled its location.

The side of the fibril, with further retraction of the probe, simply peeled against the probe surface from its prone state. The fibril did not reach a buckled state again. Hence, prior to fibril detachment, when the distance between the probe and the backing layer was approximately equal to the length of the micropillar, most of the side contact between the fibril and the probe had been eliminated by peeling and the remaining compressive stress was negligible. The small remaining area of the side of the fibril, with no remnant tip contact (or compressive stress), peeled-off the probe surface very easily so that negligible tension was needed for detachment. Thus, it appears that tip contact re-formation during fibril unbuckling is crucial for any adhesion during final detachment.

Comparison to Euler Buckling Theory

Figure 11 shows the compressive stress on a fibril at buckling and unbuckling; the data points were obtained as averages from several repetitions of the experiments.

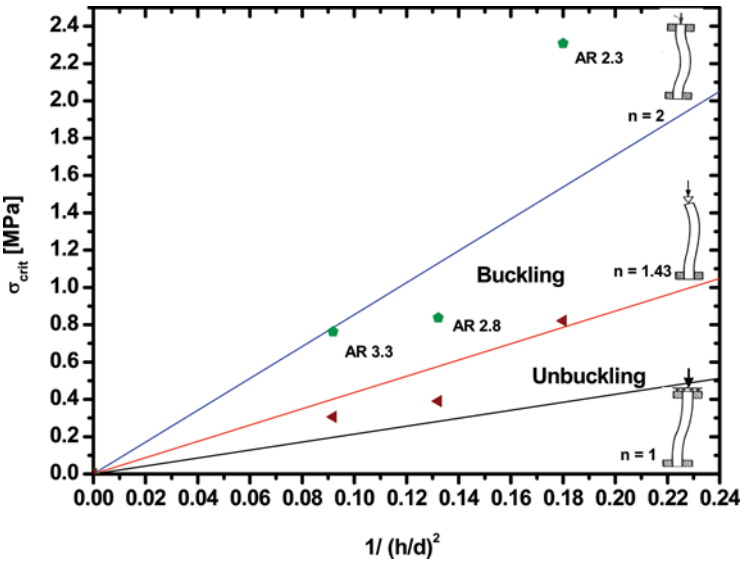

FIGURE 11 Experimental data (symbols) for the stress at buckling (green diamond) and unbuckling (red triangles) for single micropillars as a function of $(1/AR)^2$, where AR is the aspect ratio d/h. Also shown are the theoretical results (lines) for Euler buckling under three different combinations of boundary conditions, as illustrated in the thumbnail sketches. A value of E = 3.4 MPa was used, measured experimentally during compression of single micropillar specimens (error for at least three different measurements for each data point was found to be within the size of the symbols) (color figure available online).

The stress is plotted *versus* $(d/h)^2$, i.e., $(1/AR)^2$, because of the scaling that occurs in the Euler buckling formula as discussed below. As expected, the fibrils with the highest AR buckle at the lowest stress. The trend is similar in the case of unbuckling. We note that the stress at which unbuckling occurs is considerably smaller than that at which buckling takes place.

To model the buckling and unbuckling load, we assume that the fibril can be treated as a slender column; such an assumption is not entirely justifiable, as a slender column would have an AR > 7, whereas the most slender fibrils in the present work had AR = 3.3. Nevertheless, we use the slender column assumption because relevant results for the buckling of a stocky column representative of the fibrils sitting on a backing layer are scarce. The critical stress for buckling was calculated using the following equation [28]:

$$\sigma_{crit} = \frac{n^2\pi^2 E_{avg}}{16}\left(\frac{1}{AR}\right)^2, \tag{2}$$

where n is a pre-factor that depends on the end condition/restraint on the buckling pillar, AR = d/h where d is the diameter and h the height of the micropillar, and E_{avg} is the elastic modulus. The value of the modulus was

determined using Eq. (1) as described above, with an important exception that the measurement of the total compliance was based on the *linear compressive regime* of the load-displacement curve prior to buckling. It was found that the modulus for the compressive regime, with an overall average of 3.46 ± 0.086 MPa, was higher and less scattered than that determined previously from the tensile regime.

The predictions from Eq. (2) are plotted in Fig. 11 as straight lines with slopes that depend on the value of n. Plots have been provided for three cases, where, for simplicity, the fibril base at the backing layer in all situations was assumed to be constrained against rotation; this assumption may not be exactly valid due to a compliant backing.

For the case of $n = 1$, the fibril tip, adhered to the probe, is constrained not to rotate but can translate freely sideways. In another case, the constraint against rotation of the fibril tip is retained and it is also hindered to move sideways, giving a value $n = 2$. An intermediate case is also considered, where the fibril tip, adhered to the probe, is free to rotate, but not capable of translating sideways, so that $n = 1.43$ [28]. The mode of buckling in each case is illustrated by a thumbnail sketch in Fig. 11.

Experimental buckling loads appear to correlate most closely with the clamped-clamped ($n = 2$) prediction, though the correlation is somewhat weak. In addition, the load at which unbuckling occurs would seem to correlate best with the clamped/free-to-rotate prediction ($n = 1.43$), though, again, the correlation is rather weak. Furthermore, the stockiest fibril (AR = 2.3) buckles at a load significantly higher than the clamped-clamped prediction, which may be attributed to the limitation discussed above. For this micropillar, the Euler equation predicts that an axial compressive strain at the critical buckling load of almost 50%. As a consequence, the fibril diameter will have increased by approximately 40%, making the micropillar significantly harder to buckle. Its AR at the critical stress was decreased almost by a factor of three, which further supports a critical stress in excess of the Euler prediction.

The correlation between buckling and prediction from the clamped-clamped model, and of unbuckling with the clamped/free-to-rotate case, is consistent with comments of Glassmaker *et al.* [22] and with the recent insights of Stark et al. [30]. The latter considered Euler buckling of a fibril clamped at its bottom end and adhering to a platen at its tip. In their case, the platen was free to translate sideways, and thus, in the absence of tip detachment, behaved like the case of $n = 1$. Stark *et al.* [30] found that buckling initiated at the load consistent with the critical load for a column fully adhered at its tip, *i.e.*, at the level predicted by the case of $n = 1$. Such a response arises because when buckling commences under rising compressive load magnitude, the tip adhering to the platen is in compression everywhere at the moment buckling sets in, and thus is not free to rotate. In our experiments the probe to which the fibril tip is adhered is not free to translate

sideways. We deduce from this that buckling of an adhered fibril under rising compressive load magnitude will occur at the critical load consistent with the clamped-clamped case ($n = 2$) illustrated in Fig. 11. The fibril tip will be in compression everywhere at the instant when buckling commences and will neither be free to rotate nor translate sideways. To the extent that the Euler buckling model is relevant to our stocky fibrils, it is thus consistent that the buckling in the experiments correlates most closely with the line for the clamped-clamped case.

Stark *et al.* [30] further deduced from their modelling that shortly after buckling occurs under rising compressive load, detachment of the fibril tip from the platen begins due to the tension that develops on one side of the contact because of the bending of the fibril during buckling. This process continues until only a small fraction of the fibril tip is in contact with the platen, and, simultaneously, the compressive load drops dramatically. When the platen is retracted, the compressive load relaxes and the buckled fibril then sits with its tip only partially adhered to the platen. Because of that condition the fibril tip is relatively free to rotate, so that unbuckling can occur in conditions that are best modelled by the clamped/free-to-rotate case ($n = 1.43$) illustrated in Fig. 11. Therefore, in our experiments we can expect that unbuckling occurred at a load close to that predicted by the clamped-free to rotate case ($n = 1.43$). The experimental data for unbuckling agree fairly well with this prediction.

CONCLUSIONS

Buckling of adhesive single micropillars of PDMS was investigated. This study showed that:

- The adhesion of single micropillars and their stiffness generally *increased* with a *decrease* in their aspect ratio.
- The round edge of the fibrils influenced the adhesion strength by acting as a circumferential defect.
- *Reversible* buckling, assisted by the residual area of the tip that remains in contact with the probe in the buckled state, ensured contact re-formation against a probe with a large radius of curvature. The compressive state of stress that prevailed after unbuckling also aided in the formation of a strong re-attachment. A slight drop in adhesion was attributed to adhesion hysteresis.
- *Irreversible* buckling occurred when the fibril slipped during unloading under a probe having a small radius of curvature. Thereafter, the micropillar simply peeled against the probe in side contact without any reversal of the buckled state. Lack of tip contact re-formation was responsible for substantial loss of adhesion in this case.

- Buckling of fibrils appears to follow the predictions of Euler buckling theory; higher aspect ratio fibrils buckled at lower compressive stress. During buckling the pillar acted as one clamped at the base as well as at the top. During unbuckling the tip was relatively free to rotate, and the fibril unbuckled at a lower compressive stress magnitude than that which caused buckling.
- The understanding of the mechanisms of contact re-formation during reversible and irreversible buckling may provide help in the effort to design a switchable, fibrillar adhesive system exploiting the mechanical instability.

A single microscale fibril with a tilt with respect to the horizontal has been used for pick-and-place manipulation of micrometer-scale silicon microplatelets and glass cover-slips [31]. An array of fibrils also shows similar effects on adhesion induced by mechanical instability along with the dominating role of statistical distribution of contact force. This effect has been used to develop simple applications for pick-and-place of an object [24].

ACKNOWLEDGMENT

We thank Anand Jagota for insightful discussions and Chelsea Davis for her support on adhesion testing. This work, as part of the European Science Foundation EUROCORES Program FANAS, was supported by the German Science Foundation (DFG) grant AR201/9-1. M.D.B. and A.J.C. acknowledge the National Science Foundation Materials Research Science and Engineering Center (NSF-DMR 0820506) for financial support.

REFERENCES

[1] Kamperman, M., Kroner, E., del Campo, A., McMeeking, R. M., and Arzt, E., *Adv. Eng. Mater.* **12**, 335–348 (2010).
[2] Boesel, L. F., Greiner, C., Arzt, E., and del Campo, A., *Adv. Mater.* **22**, 2125–2137 (2010).
[3] Jagota, A. and Hui, C. Y., *Mat. Sci. Eng. R.* **72**, 253–292 (2011).
[4] Hui, C. Y., Jagota, A., Bennison, S., and Londono, J., *P. Roy. Soc. Lond. A Mat.* **459**, 1489–1516 (2003).
[5] Persson, B. N. J., *J. Chem. Phys.* **118**, 7614–7621 (2003).
[6] Kim, S., Sitti, M., Hui, C. Y., Long, R., and Jagota, A., *Appl. Phys. Lett.* **91**, 161905 (2007).
[7] Long, R., Hui, C. Y., Kim, S., and Sitti, M., *J. Appl. Phys.* **104**, 044301–044309 (2008).
[8] Bartlett, M. D., Croll, A. B., King, D. R., Paret, B. M., Irschick, D. J., and Crosby, A. J., *Adv. Mater.* **24**, 1078–1083 (2012).
[9] del Campo, A., Greiner, C., and Arzt, E. *Langmuir* **23**, 10235–10243 (2007).

[10] Gao, H. and Yao, H., *Proc. Natl. Acad. Sci.* **101**, 7851–7856 (2004).
[11] del Campo, A. and Greiner, C., *J. Micromech. Microeng.* **17**, R81–R95 (2007).
[12] Aksak, B., Hui, C. Y., and Sitti, M., *J. R. Soc.: Interface* **8**, 1166–1175 (2011).
[13] Kroner, E., Paretkar, D. R., McMeeking, R. M., and Arzt, E., *J. Adhesion* **87**, 447–465 (2011).
[14] Persson, B. N. J. and Gorb, S., *J. Phys. Chem.* **119**, 11437–11444 (2003).
[15] Cañas, N., Kamperman, M., Völker, B., Kroner, E., McMeeking, R. M., and Arzt, E., *Acta Biomater.* **8**, 282–288 (2012).
[16] Vajpayee, S., Jagota, A., and Hui, C. Y., *J. Adhesion* **86**, 39–61 (2010).
[17] Tang, T., Hui, C. Y., and Glassmaker, N. J., *J. R. Soc.: Interface* **2**, 505–516 (2005).
[18] Spuskanyuk, A. V., McMeeking, R. M., Deshpande, V. S., and Arzt, E., *Acta Biomater.* **4**, 1669–1676 (2008).
[19] Guidoni, G. M. M., Schillo, D., Hangen, U., Castellanos, G., Arzt, E., McMeeking, R. M., and Bennewitz, R., *J. Mech. Phys Solids* **58**, 1571–1581 (2010).
[20] Autumn, K., Dittmore, A., Santos, D., Spenko, M., and Cutkosky, M., *J. Exp. Biol.* **209**, 3569–3579 (2006).
[21] Paretkar, D., Schneider, A. S., Kroner, E., and Arzt, E., *MRS Comm.* **1**, 53–56 (2011).
[22] Glassmaker, N. J., Himeno, T., Hui, C. Y., and Kim, J., *J. R. Soc.: Interface* **1**, 23–33 (2004).
[23] Hui, C. Y., Jagota, A., Shen, L., Rajan, A., Glassmaker, N., and Tang, T., *J. Adhesion Sci. Tech.* **21**, 1259–1280 (2007).
[24] Paretkar, D., Kamperman, M., Schneider, A. S., Martina, D., Creton, C., and Arzt, E., *Mat. Sci. Eng. C-Bio. S.*, **31**, 1152–1159 (2011).
[25] Greiner, C., del Campo, A., and Arzt, E., *Langmuir* **23**, 3495–3502 (2007).
[26] Jagota, A. and Bennison, S., *Integr. Comp. Biol.* **42**, 1140–1145 (2002).
[27] Anderson, T. L., *Fracture Mechanics: Fundamentals and Applications*, (CRC Press, Inc., 2000)., Ch. 2, pp. 59–61.
[28] Timoshenko, S. P. and Gere, J. M., *Theory of Elastic Stability*, 2nd ed., (McGraw-Hill, New York and London, 1961)., Chap. 2, pp. 47–50.
[29] Chaudhury, M. K. and Whitesides, G. M., *Langmuir* **7**, 1013–1025 (1991).
[30] Stark, S., Begley, M. R., and McMeeking, R. M., *J. Appl. Mech.* (n.d.).
[31] Mengüc, Y., Yang, S. Y., Kim, S., Rogers, J., and Sitti, M., *Adv. Funct. Mater.* **6**, 1246–1254 (2012).